Chalcogenide Letters Vol. 18, No. 4, April 2021, p. 215 - 224

Investigations of crystallization kinetics and phase transformation of 1000 nm of $Ge_{20}Sb_{20}Te_{60}$ thin film from electrical measurements

E. R. Shaaban[a,*], H. I. Elsaeedy[b], Mona Mahmoud[b], Said A. Abdelaal[c], H. A. Yakout[b], Abdelaziz M. Aboraia[a,d]

[a]*Physics Department, Faculty of Science, Al-Azhar University, P.O. 71452, Assiut, Egypt*

[b]*Department of Physics, Faculty of Science, King Khalid University, Abha, Kingdom of Saudi Arabia*

[c]*Department of Chemistry, Faculty of Science, Jazan University, Saudi Arabi.*

[d]*The Smart Materials Research Institute, Southern Federal University, Sladkova 178/24, 344090, Rostov-on-Don, Russia*

In this work we will focus first on obtain the sheet resistance, R_s of thin film whose surface thickness is equal to 1000 nm for the chalcogine $Ge_{20}Sb_{20}Te_{60}$ at different heating rates , this is done against temperature in the range from 70 to 370 °C. The sheet resistance curve and through derivation of sheet resistance as a function of temperature there was clearly evidence of two crystallization regions for the studied sample. Second, the thermal data we obtained was used to complete the thermal calculations and then the electrical calculations thereafter. The activation energies of crystallization were evaluated by kinetic criteria. The activation energy, E_c, and Avrami index, n, were obtained by analyzing the data via JMA methods. The results indicated that the transformation from amorphous to crystalline phases. The crystalline phases for the as-deposited and annealed film were identified via x-ray diffraction (XRD).

(Received March 6, 2021; Accepted April 21, 2021)

Keywords: Sheet resistance, $Ge_{20}Sb_{20}Te_{60}$; Thin films, Thermal properties, Crystallization kinetics

1. Introduction

Few decades ago, phase change of chalcogenides have great attention for next-generation non-volatile memory [1–3] and high density optical recording [4–7]. Typically, a chalcogenides possess two or more separately states at which it displays distinguishable material properties. Phase-change materials (PCMs) have attracted intensive interests, because they offer large optical and electrical contrast between amorphous and crystalline phases in combination with rapid and reversible switching between these two phases and with excellent prospects for down-scaling. The significant difference between these states in electrical and optical properties upon the reversible switching allows storing the rewritable digital bit information [8-10]. With developments in lithography and discoveries in chalcogenide compounds, recently GST emerged as an important candidate for the electronic nonvolatile memory devices [10–14]. Many binary compounds can be synthesized by associating one of the chalcogene with another element of the periodic table like, indium, antimony, copper and silicon, etc [15-17]. The binary chalcogenide amorphous alloys Ge-Te and Sb-Te are important form both the scientific and industrial points of view due to their phase-change properties and application as a basic system in recording materials of phase change optical disks [18-20]. It is note that the addition of Sb to Ge-Te increase the practicality of commercial-scale production by easing the requirement for precision in the composition of

* Corresponding author: esam_ramadan2008@yahoo.com

deposited film without deleterious effect in the stability [21]. This framework introduces thermal and electrical properties in a new format without the need for procedure thermal measurements from bulk material. The same is true for electrical properties. In the present work, the calculations of both the thermal and the electrical parameters have been determined in terms of measuring the sheet resistance as a function of temperature of the thin film at different heating rates. The crystallized phases were verified over the temperature that applied to the thin films by the XRD.

2. Experimental methods

Bulk chalcogenide $Ge_{20}Sb_{20}Te_{60}$ sample was prepared according to the conventional melt-quenched technique. The high-purity of the constituent elements Ge, Sb, Te elements were weighed based on their atomic percentages, using an electrical balance type (Sartorius) with accuracy ($\pm 10^{-4}$ g) and sealed in evacuated silica tubes (10^{-5} Torr) and it was heated at 1200 ^{o}C for 24 hours. After the synthesis, the melt was quenched in water at 273 K to obtain the $Ge_{20}Sb_{20}Te_{60}$ glassy alloy. Then, the powdered sample was prepared by grinding of the resulting bulk alloy sample in a mortar whereas the thin film of $Ge_{20}Sb_{20}Te_{60}$ was deposited onto well-cleaned glass substrate at room temperatures by thermal evaporation technique using a high vacuum coating unit (Edward E 306A, UK). The thickness of the studied film was kept ~ 1000 nm. In order to achieve homogenous and smooth films, the substrates were rotated slowly at speed of 3 rev/min. Also, through the evaporation treatment the thickness of the formed films were monitored by using quartz crystal thickness monitor (Model FTM4, Edwards Co., UK). The structure and phase purity of the film samples were done at room temperature by X-ray diffractometer (XRD, Philips X-ray diffractometry 1710), with Ni-filtered CuK_{α} radiation (λ = 0.15418 nm). The elemental composition of the $Ge_{20}Sb_{20}Te_{60}$ films were analyzed by using energy dispersive X-ray spectrometer unit (EDXS) interfaced with a scanning electron microscope (SEM, JOEL XL) operating an accelerating voltage of 30 kV, used for the morphology studies. The relative error of elements determination does not exceed 2%, during the analysis. The electrical resistivity at different heating rates was measured at room temperature by measuring currents against applied voltage using the four-probe technique. The coplanar circular Molybdenum (Mo) metal contacts were deposited on the front face of the films surfaces in a square geometry (5.0 mm) by thermal evaporation technique. The current was measured by a digital picoammeter (DPM-111 Scientific Instruments, Roorkee).

3. Results and discussion

3.1. Temperature dependent sheet resistance, R_s

The experimental relationship between sheet resistance, R_s, with temperature of the $Ge_{20}Sb_{20}Te_{60}$ film at the different heating rates, (5, 10, 15, 20 and 25 °C/min) is illustrated in Fig. 1. These measurements of the heat treatment film were performed to deduce thermal properties based on electrical measurements on the thin film without making thermal measurements of the bulk material.

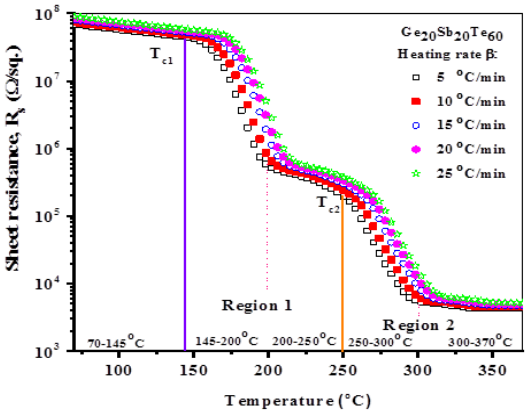

Fig. 1. Relationship between sheet resistance, R_s, and temperature, T, of the $Ge_{20}Sb_{20}Te_{60}$ thin film at different heating rates.

The curves in Fig. 1 can be divided into several stages. The temperature range of the first stage is from 70 °C to below T_{c1}, in this stage, the arrangement of atoms is not clearly changed with temperature, and therefore, the R_s decreases gradually in this temperature range but slowly. In this region, the state of the studied film is amorphous and the arrangement of atoms is random, causing its high R_s. When the temperature is increased above T_{c1}, namely, in the range (145-200 °C) the atoms have sufficient energy to rearrange. The arrangement of atoms is ordered such that the film is transformed from amorphous to crystalline state and the R_s rapidly decrease; this is the second stage. As the temperature is below T_{c2}, namely, in the range (200-250 °C) the values of R_s decrease slowly with increasing temperature. The third stage which extends from 200 °C to below T_{c2} (as shown in Fig. 1), and we obtain that R_s is low in this stage. The same explanation is repeated from T_{c2} to the last studied temperature range, namely, in two range (250-300 °C) and (300-370 °C). The obtained values for T_{c1}, T_{c2}, T_{p1} and T_{p2} are tabulated in Table 1.

Table 1. Maximum crystallization rate $(d\chi/dt)$, temperatures of crystallization (T_{c1}, T_{c2}), top crystallization temperatures (T_{p1}, T_p), kinetic exponent, n, and crystallization activation energy, E_{C1}, E_{C2} according to method of Matustia for $Ge_{20}Sb_{20}Te_{60}$ thin film at different heating rates.

β [℃ / min]	$(\frac{d\chi}{dt})_p \times 10^3 (\min^{-1})$		T_c		T_p		n		E_C	
	$(\frac{d\chi}{dt})_1 \times 10^3 (\min^{-1})$	$(\frac{d\chi}{dt})_2 \times 10^3 (\min^{-1})$	T_{c1}	T_{c2}	T_{p1}	T_{p2}	$n(1)$	$n(2)$	$E_C(1)$	$E_C(2)$
5	5.509	4.622	146	250	164	258	2.022	1.672	129.13	105.70
10	10.37	8.89	151	255	169	263	2.021	1.671	156.38	130.61
15	14.528	12.77	157	261	175	269	2.024	1.674	170.18	149.69
20	18.714	16.644	160	264	178	272	2.023	1.673	175.01	172.19
25	22.602	20.329	167	267	181	275	2.021	1.671	214.63	176.75

The contemplator for the sheet resistance and the X-ray curves see eye view that the X-ray curve supports, with all strength, the sheet resistance curve with respect to the temperature of crystalline transformation. On the other hand, derivation of the sheet resistance, R_s of the first degree relative to the temperature will lead us to know the first pillar of thermal studies.

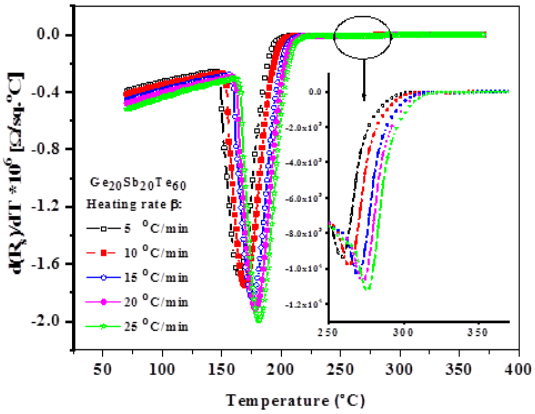

Fig. 2. Relationship between derivative of sheet resistance, dR_s/dT *and temperature, T, of the* $Ge_{20}Sb_{20}Te_{60}$ *thin film at different heating rates.*

Fig. 2 shows the relationship between derivative of sheet resistance, dR_s/dT and temperature, T. Now, the exothermic heat flow is given by:

$$\Delta Q_{exo} = -[\frac{dR_s}{dT}]_{endo.} \tag{1}$$

Fig. 3 (a, b) represents the exothermic heat flow and the fraction, χ, crystallized at a given temperature, T, for heating rate equal to 5 °C/min, which given by $\chi = A_T/A$, where A is the total area of the exothermic between the temperature, T_i, where crystallization is just beginning and the temperature, T_f, where the crystallization is completed, A_T is the area between T_i and T.

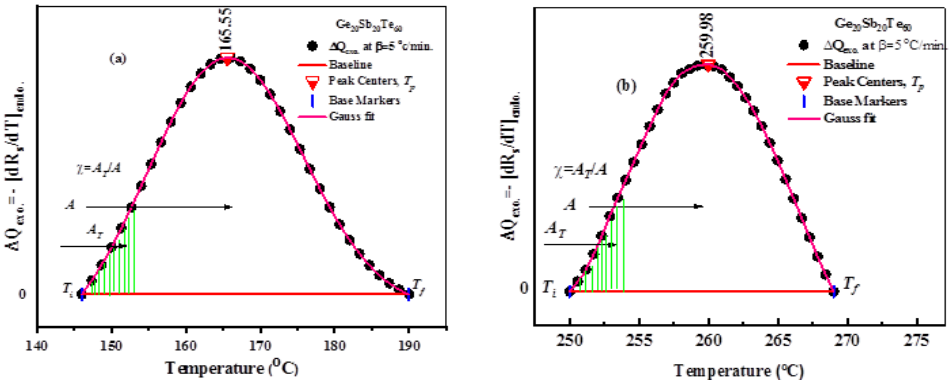

Fig. 3 (a, b). The exothermic heat flow and the fraction, χ, crystallized at a given temperature, T, for heating rate equal to 5 °C/min of the $Ge_{20}Sb_{20}Te_{60}$ *thin film at different heating rates.*

The graphical representation of the volume fraction crystallized, χ appears the typical sigmoid curve as a function of temperature at different hating rates for studied sample as shown in Fig. 4 (a, b) and gives by:

$$\chi = \sum_{i=0}^{s} \Delta Q_{exo} / \sum_{i=0}^{99} \Delta Q_{exo} \tag{2}$$

where s is number of points of ΔQ_{exo}, (namely, s = 0 to 99). From Fig. 4 (a, b), we notice a systematic shift in χ to higher temperature with increase of the heating rate β.

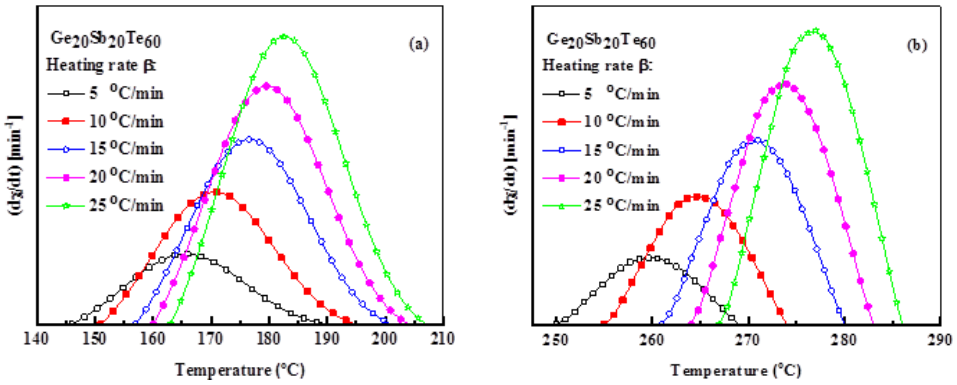

Fig. 4 (a, b): Maximum crystallization rate, $(d\chi/dt)_p$ versus temperature, T, of the exothermal peaks for the $Ge_{20}Sb_{20}Te_{60}$ thin film at different heating rates.

The ratio between the ordinates of the ΔQ_{exo} curve and the total area of the peak gives the corresponding crystallization rates $(d\chi/dt)_p$, which makes it possible to build the curves of the exothermal peaks represented in Fig. 5. It may be observed that, the $(d\chi/dt)_p$ values increases as well as the heating rate, a property that has been widely discussed in the literature [22].

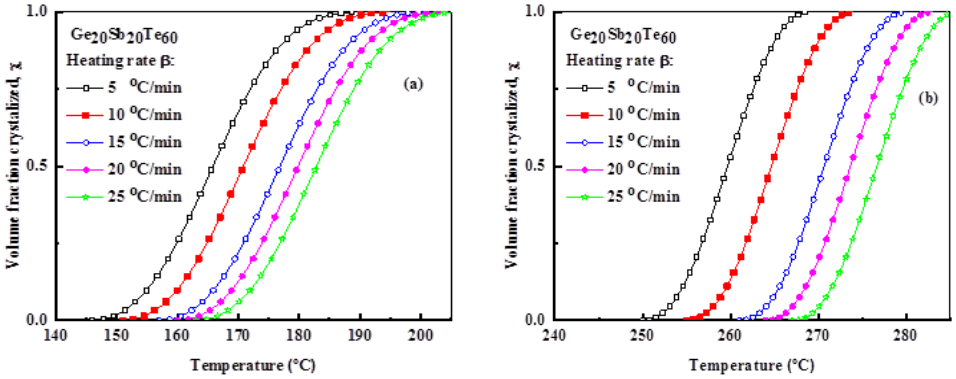

Fig. 5 (a, b). The typical sigmoid curve of the volume fraction crystallized, χ, as a function of temperature, T, for the $Ge_{20}Sb_{20}Te_{60}$ thin film at different heating rates.

3.2. Evaluation of the activation energy

There are several methods to compute the activation energy of amorphous-crystalline transformation, E_c, the Avrami exponent, n, the frequency factor, K_0, and constants for the investigated glass. Both the methods of Kissinger and Matusita [23] were addressed in this work.

3.2.1. Method of Kissinger

The activation energy E_c of amorphous-crystalline transformation was originally computed via the relation derived by Kissinger [24] as:

$$\ln\left(\beta/T_p^{\,2}\right) = -E_c/RT_p + \ln(E_c/RK_0) \tag{3}$$

Fig. 6 represents the plots of $\ln\left(\beta/T_p^{\,2}\right)$ versus $(1000/T_p)$ for the studied sample. The plots were found to be straight lines. The activation energy, E_c, and frequency factor, K_0, are then computed by least squares fitting method. The values for both E_c and K_0 equal to 19.77 Kcal/mole, 9.4×10^5 for T_{p1} and 49.64 Kcal/mole, 5.42×10^9 for T_{p2}, respectively.

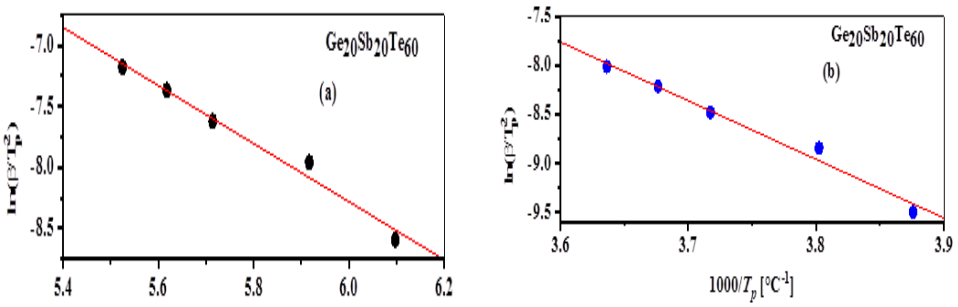

Fig. 6 (a, b). The plot of $\ln\left(\beta/T_p^{\,2}\right)$ *versus* $(1000/T_p)$ *for* $Ge_{20}Sb_{20}Te_{60}$ *thin film at different heating rates.*

On the other hand, the reaction rate constant or the kinetic parameter has a temperature dependency based on the Arrhenius equation:

$$K(T) = K_0 \exp[-\frac{E_c}{RT}] \tag{4}$$

where E_c is the effective activation energy for crystal growth, K_0, is the pre-exponential factor (the frequency factor) and *R* is the gas constant. In addition, a kinetic parameter, *K(T)*, with Arrhenian temperature dependence, is submitted to the stability criteria. According to Surinach *et al*. [25] and Hu and Jiang [26] the thermal stability of glassy materials estimates via the following criterion as:

$$K(T_p) = K_0 \exp[-\frac{E_c}{RT_p}] \tag{5}$$

The value of this criterion allusive the tendency of glass to devitrify on heating, whereas the glass formation is a kinetic process. The $K(T_p)$ as a function of T_p for the studied sample is shown in Fig. 7 (a, b).

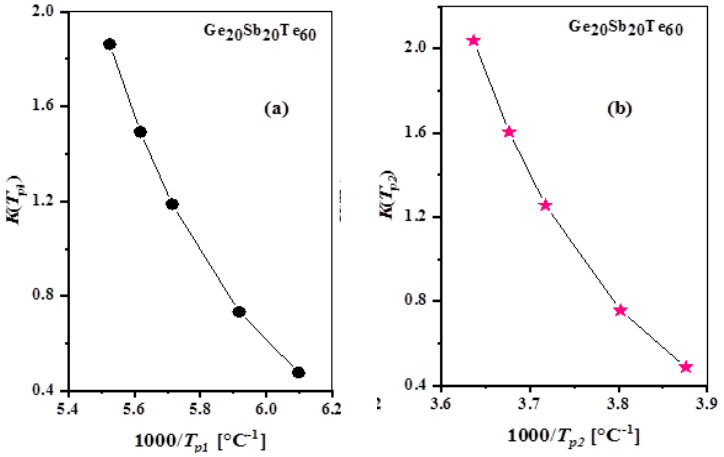

Fig. 7 (a, b). The plot of $K(T_p)$ *as a function of* T_p *for* $Ge_{20}Sb_{20}Te_{60}$ *thin film at different heating rates.*

Furthermore, from the experimental values of the $(d\chi/dt)_p$ one can computed the kinetic exponent *n* via the following equation:

$$(d\chi/dt)_p = \frac{n(0.37\beta E_c)}{RT_p^2} \tag{6}$$

The *n* values for investigated sample are computed and listed in Table 1. Finally, the experimental data, T_p, and $(d\chi/dt)_p$, shown also in Table 1 and the values of the activation energy of crystallization process for the crystallization peaks which get from Kissinger method in both crystallization regions (19.77 Kcal/mole and 49.64 Kcal/mole, respectively), make it possible to computed, through Eq. (6), the kinetic exponent, *n*, for each of the experimental heating rates for the peaks for investigated sample, whose values are also tabulated in Table 1. The kinetic exponent, *n*, was determined according to the mechanism of crystallization. Mahadevan *et al.* [27] have shown that *n* may be 4, 3, 2, which are related to different glass-crystal transformation mechanisms: *n* = 4, volume nucleation, three-dimensional growth; *n* = 3, volume nucleation, two-dimensional growth, *n* = 2, volume nucleation, one-dimensional growth; *n* = 1, surface nucleation, one-dimensional growth from surface to the inside. Therefore, bearing in mind the above obtained mean value, $\langle n \rangle$ = 2.02 and $\langle n \rangle$ = 1.67 for two crystallization regions (as shown in Table 1) means volume nucleation, one-dimensional growth at *n* equal to 2.02. The computed *n* values are not integers. This means that the crystallization occurs by more than one mechanism [28, 29].

3.2.2. Method of Matusita

Furthermore the activation energy, E_c, of the investigated sample was computed via the Matustia relationship [30]:

$$\ln(-\ln(1-\chi)) = -n\ln\beta - 1.052\frac{mE_c}{RT} + const. \tag{7}$$

where (*m* = *n*-1) is the dimension order parameter and (*n*) is constant related to the crystallization mechanism. Fig. 8 (a. b) plots $\ln(-\ln(1-\chi)$ versus $1000/T$ at different heating rates for the studied sample. For the computation of E_c we take into consideration the linear region of this

plot. From the average, n values and $mE_c(n=m+1)$, the effective activation energies, E_c, for the studied sample is computed and listed in Table 1, where they are referred to E_{c1} and E_{c2} to indicate the two crystallization regions.

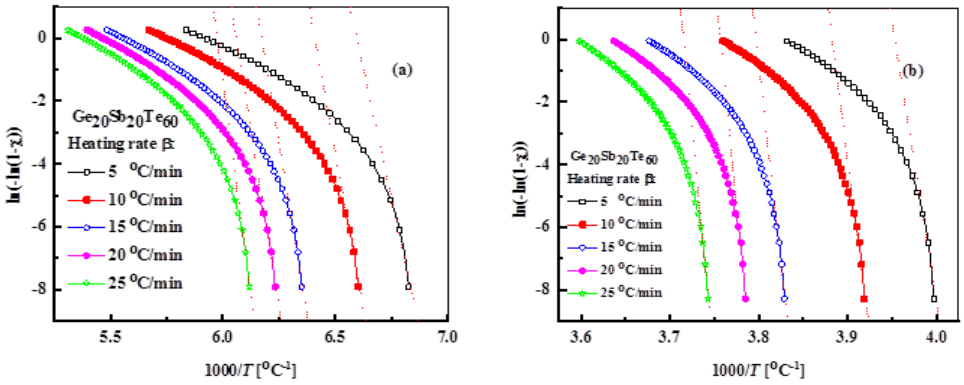

Fig. 8 (a, b). The plot of $\ln(-\ln(1-\chi)$ *versus* $1000/T$ *for* $Ge_{20}Sb_{20}Te_{60}$ *thin film at different heating rates.*

4. Identification of the crystalline phases

The amorphous/crystalline nature of the studied as-prepared $Ge_{20}Sb_{20}Te_{60}$ thin film was confirmed via X-ray diffraction (XRD) measurements as presented in Fig. 9 (a). The absence of any peak in the XRD scan of the as-prepared film confirms its amorphous nature. But, the diffractogram of an annealed films at 169 °C and 263 °C show sharp peaks as shown in Fig. 9 (b, c).

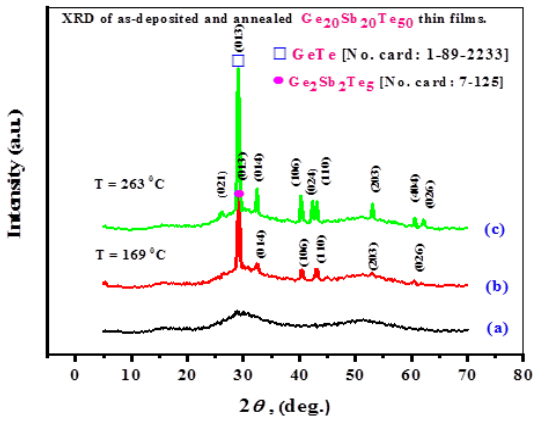

Fig. 9. X-ray diffraction pattern of as-prepared and annealed $Ge_{20}Sb_{20}Te_{60}$ *thin films.*

These sharp peaks indicate the development of amorphous structure along with ploy-crystalline phases during the heat treatment of studied film. The diffraction of dominant peaks were indexed with GeTe phase [No.card:7-125] for an annealed film at 169 °C and $Ge_2Sb_2Te_5$ phase [No.card:1-89-2233] for an annealed film at 263 °C along their respective 2θ value (JCPDS database, 1998) as presented in Fig. 9 (b, c). It can also be seen that the crystallite size, D, increases in annealed films estimated with Scherrer's formula:

$$D = \frac{0.94\lambda}{\beta \cos(\theta)} \tag{8}$$

where D is the crystallite size, λ is the wavelength of CuKα (λ = 0.15405 nm), β is the FWHM in radians computed for the highest intensity peak in the XRD scan and θ is the diffraction angle in the range (5° - 70°). The average size of the crystallites at the dominant peak for the annealed films at 169 °C and 263 °C was estimated at about 44.32 and 57.39 nm, respectively according to Eq. (8).

5. Conclusions

The structural, thermal and electrical properties of thermally evaporated thin film (1000 nm) of $Ge_{20}Sb_{20}Te_{60}$ at different heating rates have been evaluated and discussed according to sheet resistance, R_s, measurements. The R_s decreases continuously in the range (145-200 °C) until an abrupt drop shows at the temperatures of 146, 151, 157, 160 and 163 °C for corresponding heating rates (5, 10, 15, 20 and 25 °C/min), respectively, and these temperature are called the first crystallization temperature (T_{c1}), this gradient continues until it gets to the highest degree of crystallization, T_{p1} and then the sheet resistance decreases in a continuous behavior in the range (200-250 °C) until an abrupt drop shows recently at the temperatures of 250, 255, 261, 264 and 267 °C, namely, the second crystallization temperature (T_{c2}) unit this manner up to T_{p2} after that the lowest values of sheet resistance exist in the direction to the end of the range of temperature.

Then, the thermal properties and kinetics parameters such the activation energy of amorphous-crystalline transformation, E_c, the Avrami exponent, n, the frequency factor, K_0, have been determined. The amorphous/crystalline nature of the studied as-prepared $Ge_{20}Sb_{20}Te_{60}$ thin film was confirmed via X-ray diffraction (XRD) measurements.

Acknowledgments

The authors extend their appreciation to the Deanship of Scientific Research at King Khalid University, Saudi Arabia for funding this work through Research Groups Program under grant number R.G.P.1/170/41.

References

[1] M. Wuttig, N. Yamada, Nat. Mater. **6**, 824 (2007).
[2] A. V. Kolobov, P. Fons, A. I. Frenkel, A. L. Ankudinov, J. Tominaga, T. Uruga, Nat. Mater. **3**, 703 (2004).
[3] M. K. Qureshi, V. Srinivasan, J. A. Rivers, Acm Sigarch Comput. Archit. News **37**, 24 (2009).
[4] S. Raoux, W. Welnic, D. Ielmini, Chem. Rev. **110,** 240 (2010).
[5] T. H. Lee, D. Loke, K.-J. Huang, W.-J. Wang, S. R. Elliott, Adv. Mater. Deerfield Beach Fla **26**, 7493 (2014).
[6] P. Hosseini, C. D. Wright, H. Bhaskaran, Nature **511**, 206 (2014).
[7] Walter K. Njoroge, Han-Willem Wöltgens, Matthias Wuttig, Journal of Vacuum Science & Technology A: Vacuum, Surfaces, and Films **20**, 230 (2002).
[8] Bin Chen, Gert H. ten Brink, George Palasantzas, Bart J. Kooi, Scientific Reports **6**, 39546 (2016).
[9] Martin Wimmer et al., Frontiers in Physics **2**, 75 (2014).
[10] E. A. Davis, N. F. Mott, Philosophical Magazine **22**, 0903 (1970).
[11] J. K. Olson, H. Li, P. C. Taylor, Journal of Ovonic Research **11**, 1 (2005).

[12] S. El Yousef, A. El-Adawy, N. El Koshkhany, E. R. Shaaban, Journal of Physics and Chemistry of Solids **67**, 1649 (2006).
[13] Tong Ju et al., Journal of Non Crystalline Solids **354**, 2662 (2008).
[14] S. Kozyukhin. Nguyen Huy Phuc, K. D. Tsendin, Yu Prikhodko, Int J Adv Res Phys Sci, **3**, 1 (2016).
[15] E. Garcıa-Garcıa, Journal of Vacuum Science & Technology A: Vacuum, Surfaces, and Films **174**, 1805 (1999).
[16] S. Kumar, D. Singh, S. Sandhu, R. Thangaraj, Physica Status Solidi A **209**, 2014 (2012).
[17] E. R. Shaaban, Y.A. M. Ismail, H. S. Hassan, Journal of Non-Crystalline Solids **376**, 61 (2013).
[18] Afaf A. Abd El-Rahman, F. M. Hafez, F. Ahmad, M. M. Elokr, Chalcogenide Letters **91**, 41 (2012).
[19] S. H. Lee, Y. Jung, H. S. Chung, A. T. Jennings, R. Agarwal, Physica E **40**, 2474 (2008).
[20] P. Hosseini, C. D.Wright, H. Bhaskaran, Nature **511**, 206 (2014).
[19] N. F. Mott, E. A. Davis, R. A. Street, Philosophical Magazine **32**, 961 (1975).
[21] S. R. Ovshinsky, J. Non-Cryst. Solids **141**, 200 (1992).
[22] K. Matusita, S. Saka, J Non-Cryst Solids **38**(9), 741 (1980).
[23] A. Goel, E. R Shaaban, D. U. Tulyaganov, J. M. F.Ferreira, Journal of the American Ceramic Society **91**, 2690 (2008).
[24] S. Surinach, M. D. Baro, M. T. Clavagubra-Mora, N. Clavagubra, Thermochimica Acta **133**, 287 (1988).
[25] S. Surinach, M. D. Baro, M. T. Clavagubra-Mora, N. Clavagubra, Journal of Materials Science **19**, 3005 (1984).
[26] Mahadevan, Sudha, A. Giridhar, A. K. Singh, Journal of Non-Crystalline Solids **881**, 11 (1986).
[27] E R Shaaban, I.B.I. Tomsah, Journal of thermal analysis and calorimetry **105**, 191 (2011).
[28] Tanaka, Keiji, Physical Review B **39**, 1270 (1989).
[29] Matusita, Kazumasa, Takayuki Komatsu, Ryosuke Yokota, Journal of Materials Science 191, 291 (1984).
[30] Walter K.Njoroge, Han-Willem Wöltgens, Matthias Wuttig, Journal of Vacuum Science & Technology A: Vacuum, Surfaces, and Films **20**, 230 (2002).